Peroxisomal ATP-binding cassette transporters form mainly tetramers

Received for publication, December 16, 2016, and in revised form, March 3, 2017 Published, Papers in Press, March 3, 2017, DOI 10.1074/jbc.M116.772806

Flore Geillon[‡], Catherine Gondcaille[‡], Quentin Raas[‡], Alexandre M. M. Dias[‡], Delphine Pecqueur[§], Caroline Truntzer[§], Géraldine Lucchi[§], Patrick Ducoroy[§], Pierre Falson[¶], Stéphane Savary[‡], and Doriane Trompier[‡1]

From the [‡]Laboratoire Bio-PeroxIL EA7270 and [§]CLIPP-ICMUB, Université Bourgogne-Franche-Comté, 6 Bd Gabriel, 21000 Dijon, France and the [¶]Drug Resistance and Membrane Proteins Team, Molecular Microbiology and Structural Biochemistry Laboratory, Institut de Biologie et Chimie des Protéines (IBCP), UMR5086 CNRS/Université Lyon 1, 7 Passage du Vercors, 69367 Lyon, France

Edited by George M. Carman

ABCD1 and its homolog ABCD2 are peroxisomal ATP-binding cassette (ABC) half-transporters of fatty acyl-CoAs with both distinct and overlapping substrate specificities. Although it is established that ABC half-transporters have at least to dimerize to generate a functional unit, functional equivalents of tetramers (*i.e.* dimers of full-length transporters) have also been reported. However, oligomerization of peroxisomal ABCD transporters is incompletely understood but is of potential significance because more complex oligomerization might lead to differences in substrate specificity. In this work, we have characterized the quaternary structure of the ABCD1 and ABCD2 proteins in the peroxisomal membrane. Using various biochemical approaches, we clearly demonstrate that both transporters exist as both homo- and heterotetramers, with a predominance of homotetramers. In addition to tetramers, some larger molecular ABCD assemblies were also found but represented only a minor fraction. By using quantitative co-immunoprecipitation assays coupled with tandem mass spectrometry, we identified potential binding partners of ABCD2 involved in polyunsaturated fatty-acid metabolism. Interestingly, we identified calcium ATPases as ABCD2-binding partners, suggesting a role of ABCD2 in calcium signaling. In conclusion, we have shown here that ABCD1 and its homolog ABCD2 exist mainly as homotetramers in the peroxisomal membrane.

The ABCD1 transporter belongs to the D subfamily of the ATP-binding cassette (ABC)[2] transporter family and is encoded by the *ABCD1* gene (1). A large number of mutations in *ABCD1* are responsible for the most common peroxisomal disorder, which is called X-linked adrenoleukodystrophy (X-ALD) (2). Expressed at the peroxisomal membrane, ABCD1 mediates the import of saturated and monounsaturated very long-chain fatty acids (VLCFA) as CoA esters into the peroxisome for their further degradation by β-oxidation (3–5). A defect in ABCD1 results in increased levels of VLCFA in tissues and plasma (4).

Two homologs of ABCD1 that belong to the same D subfamily are expressed in the peroxisome: ABCD2 (6) and ABCD3, also called PMP70 (7). ABCD2, the closest homolog, shares the same substrate preference with ABCD1 for saturated fatty acids (FA) and monounsaturated FA (MUFA) but has a distinct substrate preference for shorter VLCFA and polyunsaturated FA (PUFA) (5, 8, 9). ABCD3 has the broadest substrate specificity because it is involved in the transport of saturated FA, unsaturated FA, branched-chain FA, dicarboxylic FA, and C27 bile acid intermediates (10, 11).

The partial overlap in substrate specificity between ABCD1 and its homologs explains their ability, upon overexpression, to compensate for ABCD1 defect (12–14). However, the basal expression levels of ABCD2 and ABCD3 are not sufficient to allow the compensation mechanisms to be efficient enough in X-ALD patients. This may be explained by the fact that ABCD2 expression mirrors ABCD1 distribution in many cell types in different tissues (15) and by the fact that ABCD3, although ubiquitously expressed (16, 17), has mainly a distinct substrate specificity (10, 11) and mediates the transport of ABCD1 substrates with less efficiency (3).

Peroxisomal ABCD transporters are half-transporters containing one nucleotide-binding domain (NBD) and one transmembrane domain as opposed to ABC full-length transporters that contain two copies of each domain. It is therefore commonly accepted that half-transporters have to dimerize to generate a minimal functional unit. The expression pattern of peroxisomal ABC transporters allows, in principle, the formation of all combinations of heterodimers. Indeed, ABCD3 is ubiquitously expressed, and although ABCD2 expression mirrors ABCD1 distribution in many cell types in different tissues, ABCD2 expression is highly inducible (18). Thus, upon stimulation, both proteins can be expressed in the same cell. Actually, the presence of both peroxisomal ABCD heterodimers and homodimers has been evidenced mainly by FRET and co-immunoprecipitation (co-IP) assays (8, 19–23). In addition, because chimeric proteins mimicking homo- and heterodimers of ABCD1 and ABCD2 are functionally active (24), one can

This work was supported by grants from the regional council of Burgundy and from the University of Burgundy. The authors declare that they have no conflicts of interest with the contents of this article.

[1] To whom correspondence should be addressed. Tel.: 33-380396202; Fax: 33-380396250; E-mail: doriane.trompier@u-bourgogne.fr.

[2] The abbreviations used are: ABC, ATP-binding cassette; DHA, docosahexaenoic acid; EGFP, enhanced green fluorescent protein; IP, immunoprecipitation; MUFA, monounsaturated fatty acid(s); NBD, nucleotide-binding domain; PUFA, polyunsaturated fatty acids; VLCFA, very long-chain fatty acid(s); X-ALD, X-linked adrenoleukodystrophy; AMP-PNP, 5′-adenylyl-β,γ-imidodiphosphate; FA, fatty acid(s); DDM, dodecyl maltopyranoside; BisTris, 2-[bis(2-hydroxyethyl)amino]-2-(hydroxymethyl)propane-1,3-diol; HB, homogenization buffer; ACN, acetonitrile.

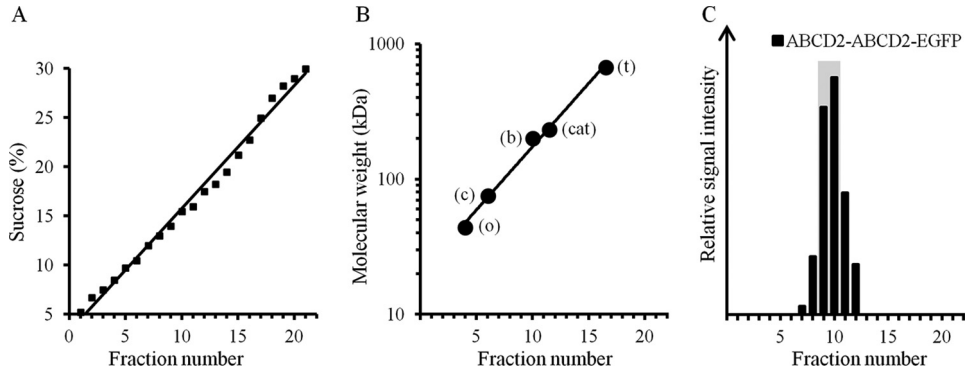

Figure 1. Calibration of velocity sucrose gradients with soluble and membrane protein markers. *A*, 5–30% (w/v) sucrose gradient linearity was checked by monitoring of sucrose concentration using a refractometer. Fractions 1–22 correspond to fractions from the top to the bottom of the gradient. *B*, calibration curve was drawn from the flotation of native soluble protein markers (*t*, thyroglobulin (669 kDa); *cat*, catalase (232 kDa); *b*, β-amylase (200 kDa); *c*, conalbumin (75 kDa); *o*, ovalbumin (44 kDa)) in parallel and equivalent sucrose gradients. *C*, ABCD2-ABCD2-EGFP (194 kDa) solubilized with 1% SDS, used as a membrane protein size marker, floated in fractions 9 and 10 (indicated by a *gray bar*) as monitored by densitometry analysis of immunoblotting performed with an anti-GFP antibody for all collected fractions.

speculate that alternative dimerization of peroxisomal ABCD transporters could lead to different substrate specificity.

It is noteworthy that the level of molecular complexity for peroxisomal ABCD half-transporters might be underestimated. Indeed, other ABC half-transporters, such as ABCG2, exhibit a tetrameric organization consisting in four core domains (25). Moreover, dimers of full-length transporters (also yielding a four-core domain organization) were observed for ABCA1 (26), ABCA3 (27), ABCC1 (28), and ABCC7 (29). Therefore, it is tempting to speculate that the interactions described within the peroxisomal ABCD subfamily occur within a higher oligomeric structure, such as a tetramer. If the substrate specificity is determined by the oligomeric status of ABCD1 and its homologs, it is essential to analyze their quaternary structure.

In this work, our objective was to study the quaternary structure of ABCD1 and ABCD2 proteins in the peroxisomal membrane by combining different biochemical approaches, including velocity sucrose gradient centrifugation, co-immunoprecipitation assays, and native PAGE. We evidenced the presence of tetrameric forms whose ABCD1/ABCD2 composition was explored and whose stability was evaluated during the catalytic cycle of the transporters. In addition, the composition of even higher molecular assemblies containing ABCD2 was deciphered by quantitative co-IP assays coupled to tandem mass spectrometry.

Results

High-molecular weight assembly of ABCD1 and ABCD2

We characterized the oligomeric state of ABCD1 and ABCD2 proteins by analyzing on a sucrose gradient the corresponding cell lysate fractions obtained by using either a denaturing detergent, such as SDS; mild detergents, such as Triton X-100, α-dodecyl maltopyranoside (α-DDM), or β-DDM; and a stabilizing detergent, C4C8 (30). Cell lysates were obtained from a specific H4IIEC3 hepatoma cell model that does not express ABCD2 at the basal level but expresses a functional ABCD2-EGFP fusion protein, depending on the dose of doxycycline added in the culture medium (clone 28.38) (8, 31). Compared with *ABCD3*, the *ABCD1* gene expression level is relatively low (31), but the ABCD1 protein expression level is sufficient to allow VLCFA β-oxidation measurements (8). At floating equilibrium, 22 fractions were collected from a 5–30% (w/v) sucrose gradient, checked for linearity (Fig. 1*A*), and calibrated with native soluble markers (Fig. 1*B*) and with a membrane protein marker (denatured ABCD2-ABCD2-EGFP; Fig. 1*C*) performed to ensure a more accurate interpretation of the results. Indeed, it should be noted that the sedimentation properties of membrane proteins depend on the amount of membrane lipids and detergent bound (size of the micelle). Thus, ABCD1- and ABCD2-particle floatation data were analyzed by considering the apparent size of the complexes based on the position of the chimeric ABCD2-ABCD2-EGFP protein marker and by considering the shift in peak positions obtained depending on the detergents.

The 22 collected sucrose fractions were analyzed by Western blotting for the presence of ABCD1 (82 kDa) and ABCD2-EGFP (111 kDa). The sedimentation of proteins solubilized with SDS was observed in fractions 6 and 7 for ABCD1 and fractions 7 and 8 for ABCD2-EGFP (Fig. 2). The molecular weights corresponding to these fractions are in agreement with a monomeric state for both ABCD1 and ABCD2-EGFP. This result was expected, considering the denaturing nature of the detergent used.

Upon solubilization with the mild detergent α-DDM, ABCD1 and ABCD2-EGFP floated as high-molecular mass complexes with a peak centered at fractions 11–14 of 215–415 kDa and at fractions 12–15 of 270–515 kDa, respectively (Fig. 2). These complexes could correspond to tetrameric associations, considering the monomeric molecular mass of ABCD1 (82 kDa) and ABCD2-EGFP (111 kDa) and the α-DDM micelle size (38.3 kDa) (32) and considering the important shift obtained from fractions 9 and 10 of the chimeric dimer ABCD2-ABCD2-EGFP (Fig. 1*C*) to the above denser fractions.

The use of detergents with intermediate strength, such as C4C8, Triton X-100, or β-DDM (Fig. 2), tended to destabilize the high-molecular weight complexes to likely dimeric forms. Indeed, upon fractionation in the presence of these detergents, ABCD1 and ABCD2-EGFP signals were found in fractions 9

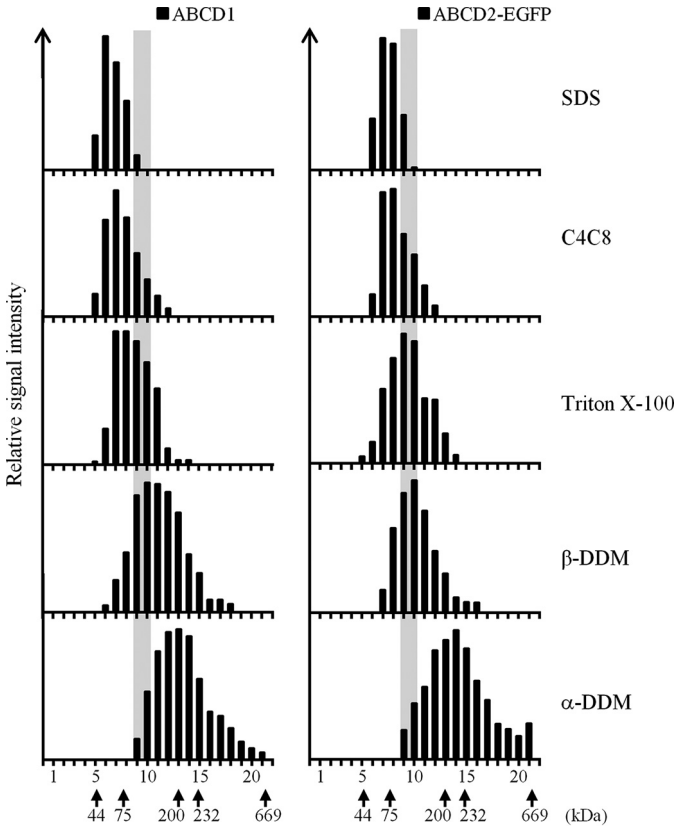

Figure 2. Velocity sedimentation of ABCD1 and ABCD2-EGFP-containing particles on sucrose gradients is dependent on the detergent used. Denatured monomeric ABCD1 and ABCD2-EGFP (from SDS lysis of induced clone 28.38) sedimented in fractions 6 and 7 and in fractions 7 and 8, respectively. In the presence of the mild detergent α-DDM, ABCD1 and ABCD2-EGFP floated as high-molecular weight complexes in fractions 11–14 of 215–415 kDa and in fractions 12–15 of 270–515 kDa, respectively. Detergents with intermediate strength (C4C8, Triton X-100, or β-DDM) destabilized these high-molecular weight complexes, considering the shift obtained to lighter fractions. The densitometric analysis of ABCD1 and ABCD2-EGFP signals detected in the gradient fractions by immunoblotting (anti-ABCD1 and anti-GFP antibodies) is given as relative signal intensity and is representative of at least two independent experiments. The positions of the soluble and membrane (position of 194-kDa ABCD2-ABCD2-EGFP indicated by a *gray bar*) protein markers are indicated.

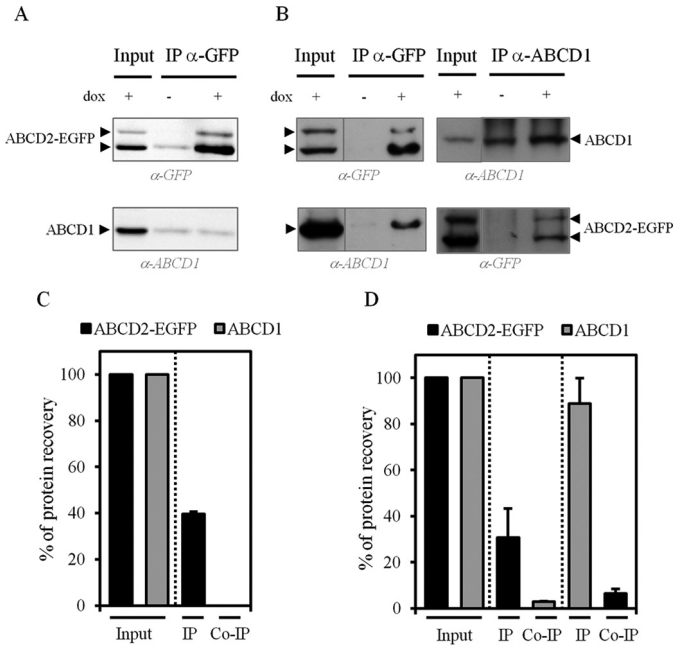

Figure 3. ABCD1/ABCD2 interaction by co-immunoprecipitation assays depends on the detergent used. Whole-cell lysates of clone 28.38 (−/+ *dox*) in the presence of 1% C4C8 (*A* and *C*) or 1% Triton X-100 (*B* and *D*) were used for anti-GFP and anti-ABCD1 IP assays. Input (one-eighth of the total amount was loaded) and eluted proteins, including immunoprecipitated and co-immunoprecipitated proteins, were analyzed by SDS-PAGE followed by immunoblotting with anti-ABCD1 and anti-GFP antibodies. *A* and *B*, immunoblots shown are representative of three independent experiments. *C* and *D*, percentage of immunoprecipitated and co-immunoprecipitated ABCD1 and ABCD2-EGFP proteins (of the input referred to as 100%). When ABCD1 and ABCD2-EGFP were solubilized in the presence of C4C8, no specific co-immunoprecipitation was detected, although a significant co-immunoprecipitation was obtained when solubilized by Triton X-100. Data are mean ± S.D. (*error bars*) ($n = 3$).

and 10, which corresponds to the position of the ABCD2 chimeric dimers (Fig. 1*C*).

Altogether, our fractionation experiments show that high-molecular weight assemblies of ABCD1 and ABCD2 are present, and their proportions were found to increase as the strength of the detergent used decreased. Upon solubilization with the milder detergent (α-DDM), the majority of high-molecular weight assemblies could correspond to tetrameric associations.

Interaction between ABCD1 and ABCD2 within supradimeric assemblies

We took advantage of the C4C8 detergent that solubilized ABCD1 and ABCD2-EGFP as a monomer/dimer mix to further characterize the dimer content. To determine whether or not heterodimers exist, we performed a cell lysis with C4C8 and immunoprecipitated ABCD2-EGFP with an anti-GFP antibody. PVDF membranes containing the immune complexes were probed with the anti-ABCD1 antibody. IP assays performed with non-induced ABCD2-EGFP lysate ("−dox" condition) were used as a control. The anti-GFP antibody immunoprecipitated ~40% of ABCD2-EGFP (Fig. 3, *A* and *C*), but no specific co-immunoprecipitation of ABCD1 was detected (when comparing *−dox* and *+dox lanes* in Fig. 3*A*), suggesting the presence of only ABCD2-EGFP within the dimer. The absence of interaction between ABCD1 and ABCD2-EGFP previously solubilized with C4C8 was further confirmed by the anti-ABCD1 IP, which failed to reveal ABCD2-EGFP in the co-IP fraction (data not shown).

However, ABCD1/ABCD2-EGFP interaction was evidenced when co-IP assays were performed on cell lysates obtained with Triton X-100, a milder detergent compared with C4C8 (Fig. 3*B*). Nevertheless, the percentage of co-immunoprecipitated ABCD2-EGFP with ABCD1 was relatively low; ABCD1 (88.8 ± 11.2% of the pool) co-immunoprecipitated only 6.4 ± 1.9% of the ABCD2-EGFP pool (Fig. 3*D*). Moreover, cross-co-IP experiments showed that a small fraction of ABCD1 was co-immunoprecipitated (2.9 ± 0.1%) with ABCD2-EGFP (30.7 ± 12.5% of the pool).

We performed quantitative cross co-IPs in BV-2 cells, a microglial cell line described to naturally express ABCD1 and ABCD2 (33). We found on one hand that the ABCD1 expression level is slightly lower in BV-2 cells than in hepatoma cells (induced clone 28.38) and, on the other hand, the expression level of the endogenous ABCD2 is comparable with the forced

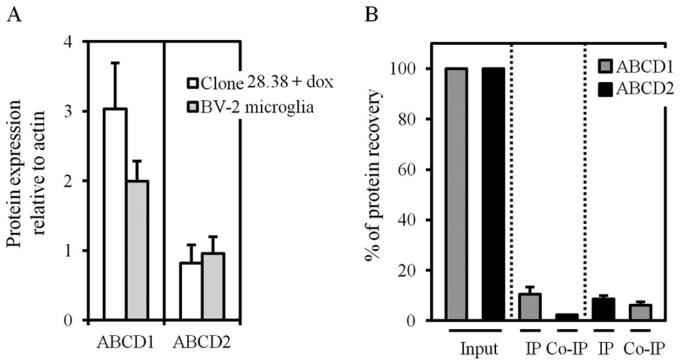

Figure 4. ABCD1 interacts with ABCD2 in the BV-2 microglial cell line. *A*, histograms showing the relative ABCD1 and ABCD2 protein expression levels as determined by densitometric analysis of immunoblots with anti-ABCD1 (*left*) and anti-ABCD2 (*right*) antibodies after normalization with actin, in mouse BV-2 cells and in rat hepatoma-induced clone 28.38. Whereas similar ABCD2 levels are found, a 1.5-fold increase in ABCD1 expression was found in BV-2 cells compared with the induced clone 28.38. Values are mean ± S.D. ($n = 3$). *B*, cross-co-IP experiments showed that ABCD1 interacts with ABCD2 in BV-2 cells. Whole-cell Triton X-100 lysates of BV-2 cells were used for anti-ABCD1 and anti-ABCD2 IP. Input and eluted proteins were analyzed by SDS-PAGE, followed by immunoblotting with anti-ABCD1 and anti-ABCD2 antibodies. Histograms show the mean percentage ± S.D. (*error bars*) of immunoprecipitated and co-immunoprecipitated proteins (out of the input referred as 100%) for three independent experiments.

expression of ABCD2-EGFP in the induced clone 28.38 (Fig. 4*A*). The analysis of repeated co-IP experiments should be approached with caution because a very low amount of immunoprecipitated ABCD1 (10.45 ± 2.8%) and ABCD2-EGFP (8.57 ± 1.5%) was obtained. Nevertheless, if we consider the above 8–10% of the immunoprecipitated proteins, ABCD1/ABCD2 interaction seems to be favored in microglial cells in comparison with hepatoma cells (induced clone 28.38). Indeed, the same overall percentage of co-IP proteins was obtained in hepatoma cells (2.9–6.4%; Fig. 3*D*) and in BV-2 cells (2.3–6.1%; Fig. 4*B*), although the percentage of immunoprecipitated proteins was much higher in hepatoma cells (30–88%; Fig. 3*D*) than in BV-2 cells (8–10%; Fig. 4*B*).

If the interaction between ABCD1 and ABCD2 or ABCD2-EGFP in ABCD2-naturally expressing cells (microglial BV-2 cells) or in ABCD2-EGFP-expressing hepatoma cells was clearly observed, it remained to evaluate whether the interaction occurs within a dimer or within higher molecular assemblies. The absence of ABCD1/ABCD2 interaction when solubilized with C4C8 and the presence of ABCD1/ABCD2 interaction when solubilized with the milder detergent Triton X-100 suggest that this interaction does not occur within a dimer but rather within supradimeric assemblies.

Homo- and heterotetrameric forms of ABCD1 and ABCD2

The fractionation experiments previously showed that ABCD1 and ABCD2-EGFP are present in high-molecular weight assemblies that could correspond to tetrameric associations.

Chimeric proteins containing two ABCD1 or ABCD2 moieties were previously reported to be functional (24). When co-expressing ABCD1 chimeric homodimers ABCD1-ABCD1 and ABCD1-ABCD1-EGFP in COS-7 cells, co-IP experiments showed that ABCD1-ABCD1 specifically interacts with ABCD1-ABCD1-EGFP, directly confirming the existence of ABCD1 homotetramers (Fig. 5*A*). The presence of ABCD2 homotetramers was confirmed as well by co-IP experiments in cells expressing ABCD2 chimeric homodimers (ABCD2-ABCD2 plus ABCD2-ABCD2-EGFP) (Fig. 5*B*). Heterotetramers as a result of an assembly of the two different homodimers ABCD1-ABCD1 and ABCD2-ABCD2-EGFP were detected similarly (Fig. 5*C*).

We further explored the ABCD1 and ABCD2 oligomeric status by native PAGE. To that end, we used a protocol for membrane proteins that we adapted by replacing glycine by histidine in the cathode buffer for sample focusing to take into account the basic character of ABCD1 and ABCD2 proteins (34). To improve the migration of membrane proteins, we used the Deriphat (disodium-*N*-lauryl-β-iminodipropionate; Anatrace)-PAGE system adapted from Peter and Thornber (35) successfully used for an ABC full-length transporter (36). The peroxisome-enriched fraction was prepared from the ABCD2-EGFP-expressing hepatoma cells (induced clone 28.38), and ABCD1 and ABCD2-EGFP were solubilized with the milder detergent α-DDM. Surprisingly, the extraction of ABCD1 and ABCD2 proteins from peroxisomal membranes by α-DDM micelles was drastically increased when peroxisomes were incubated with ATP before incubation with the detergent (Fig. 6*A*). ABCD1 and ABCD2-EGFP solubility increased from 13.7 ± 10.3 to 65 ± 9.6% and from 7.9 ± 11.4 to 43.6 ± 22.1%, respectively (Fig. 6*B*). Native electrophoresis of solubilized ABCD1 and ABCD2-EGFP proteins using the Deriphat-PAGE system resulted in a prominent band with an apparent molecular mass of ~350 kDa for ABCD1 (Fig. 6*C*) and ~480 kDa for ABCD2-EGFP (Fig. 6*D*), whereas single proteins have a molecular mass of 82 and 111 kDa, respectively. This suggests that both proteins may assemble as a tetramer. Of note, ABCD1, but not ABCD2-EGFP, was also systematically detected as a faint band at ~200 kDa consistent with dimeric assembly (Fig. 6*C*). Superimposition of the densitometric tracing of the native-PAGE electrophoretic patterns clearly showed that ABCD1 and ABCD2-EGFP were mainly present in distinct complexes, as evidenced by a weak overlapping of ABCD1 and ABCD2-EGFP bands (Fig. 6*E*).

Solubilized ABCD1 and ABCD2 from the peroxisome-enriched fraction of BV-2 cells preincubated or not with ATP (Fig. 7*A*) showed that both proteins are found in high-molecular weight complexes as well on native PAGE (Fig. 7*B*). However, both proteins were detected in broader bands with an estimated apparent molecular mass in the range of 350–700 kDa for ABCD1 (Fig. 7*B*, *left*) and in the range of 480–700 kDa for ABCD2 (Fig. 7*B*, *right*), consistent with the presence of at least tetrameric forms.

Altogether, ABCD1 and ABCD2 can form homotetramers and heterotetramers, as demonstrated by co-IP assays of chimeric dimers. Moreover, native-PAGE experiments showed that high-molecular weight assemblies for both transporters are present in BV-2 cells and in induced clone 28.38 and are likely to correspond to tetrameric associations, mainly homotetramers.

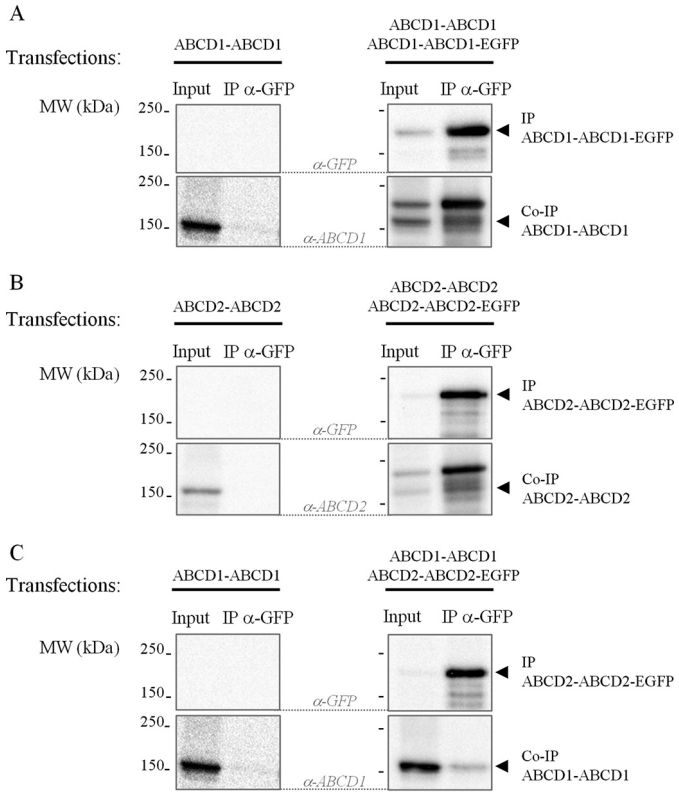

Figure 5. ABCD1 and ABCD2 are present in homo- and heterotetramers. Co-IP experiments were performed from single- and double-transfected COS-7 cells with plasmids that encode for chimeric ABCD1 dimers or chimeric ABCD2 dimers either fused to EGFP or not. Single (negative control)- and double-transfected cell lysates (400 μg) were used for the anti-GFP IP experiments. Input (50 μg) and eluted proteins (IP and co-IP proteins) were analyzed by SDS-PAGE and immunoblotting with the antibodies indicated. Immunoblots are representative of three independent experiments. *A*, using an anti-GFP antibody, co-IP of ABCD1-ABCD1 (band at ~160 kDa; *right*) with ABCD1-ABCD1-EGFP showed the presence of ABCD1 homotetramers. The anti-GFP IP performed on ABCD1-ABCD1-transfected COS-7 cells, used as negative control, revealed no band (*left*). *B*, using an anti-GFP antibody, co-IP of ABCD2-ABCD2 (band at ~160 kDa; *right*) with ABCD2-ABCD2-EGFP demonstrated the presence of ABCD2 homotetramers. No band was detected for the negative IP control (*left*). *C*, using an anti-GFP antibody, co-immunoprecipitation of ABCD1-ABCD1 (band at ~160 kDa; *right*) with ABCD2-ABCD2-EGFP showed the presence of heterotetramers. No band was detected for the negative IP control (*left panels* reused *A*).

ABCD1 and ABCD2 tetrameric assemblies remain unchanged during the catalytic cycle of the transporters

We next analyzed whether activation or inactivation of the ATP-driven fatty-acid transport assumed by ABCD1 and ABCD2 could be associated with an altered ability to tetramerize and could trap transient assembly.

Blocking ATP hydrolysis activity of ABCD1 and ABCD2 was provided by the peroxisome-enriched fraction treatment with a non-hydrolyzable competitor of ATP (AMP-PNP). Similarly to ATP, preincubation of peroxisomes with AMP-PNP drastically increased the extraction of ABCD1 and ABCD2-EGFP proteins from peroxisomal membranes by α-DDM micelles (Fig. 8*A*), indicating that nucleotide binding but not nucleotide hydrolysis is responsible for such an elevated extraction yield. Analysis of these α-DDM-soluble fractions on Deriphat-PAGE showed that ABCD1 and ABCD2-EGFP high-molecular weight assemblies (*i.e.* tetramers) remained unchanged whatever the conditions (Fig. 8*B*).

Stimulation of the ATP-driven fatty-acid transport was obtained by incubation of isolated peroxisomes in the presence of ATP, fatty acid (C26:0), and the cytosolic fraction, previously reported to be needed for functional β-oxidation in isolated peroxisomes (3). The subsequent analysis revealed a comparable ABCD1 and ABCD2-EGFP extraction efficiency in all treated samples (Fig. 8*C*) and the same banding pattern on Deriphat-PAGE (Fig. 8*D*).

Overall, by interfering with the ATP-driven fatty-acid transport assumed by ABCD1 and ABCD2-EGFP, our data indicate that ABCD1 and ABCD2-EGFP tetrameric assemblies remain unchanged during the catalytic cycle of both transporters and hence that these transporters probably form obligate tetramers.

Identification of potential ABCD2-binding partners

The asymmetric peaks seen on native-PAGE profiles with a shoulder toward the high-molecular weight region both for ABCD1 and ABCD2 (Figs. 6*E* and 7*B*) suggested that besides tetrameric forms, higher molecular assemblies of ABCD1 and ABCD2 are present (up to 720 kDa). We wondered whether ABCD1 and ABCD2 form oligomeric structures (>4 monomers) or belong to a complex formed by a tetramer interacting with other proteins.

To identify potential interacting partners specific for ABCD2, we developed a co-IP/mass spectrometry (MS) strategy. The α-DDM soluble fraction of the peroxisome-enriched fraction, prepared from the clone 28.38 expressing or not expressing ABCD2-EGFP, was subjected to anti-GFP co-IP assays. Quantitative liquid chromatography-electrospray ionization-tandem mass spectrometry was used to identify eluted proteins from co-IP assays. Differential analysis between samples expressing or not expressing ABCD2-EGFP (+dox/−dox) was performed to limit identification of false-positive interactions. Hence, only proteins detected exclusively in the positive samples were listed (Table 1). ABCD2 was successfully identified, with 26 unique peptides to ABCD2 and two shared peptides between ABCD1 and ABCD2 leading to 51.7% ABCD2 sequence coverage. Interestingly, a total of 13 non-redundant proteins were found to potentially interact with ABCD2-EGFP (Table 1). Four of them are statistically relevant (-fold change > 2): the fatty-acid amide hydrolase 1 (FAAH1), the sarcoplasmic/endoplasmic reticulum calcium ATPase 2 (AT2A2), the sodium/potassium-transporting ATPase subunit β-1 (AT1B1), and the serum paraoxonase/arylesterase 1 (PON1).

Discussion

For the first time, we demonstrate the presence of tetrameric assemblies of the peroxisomal ABCD1 and ABCD2 transporters in rodents, although the scientific community has previously reported a dimeric status for peroxisomal ABCD proteins in yeast (37, 38), rodents, or humans (8, 19–23). Our data clearly demonstrate that ABCD1 and ABCD2-EGFP are found in high-molecular weight complexes, which could correspond to tetramers, as assessed by velocity gradient centrifugation when solubilized with the mild detergent α-DDM. Tetrameric assemblies were further evidenced by co-IP assays of functional chimeric dimers expressed in transfected COS-7 cells. Opti-

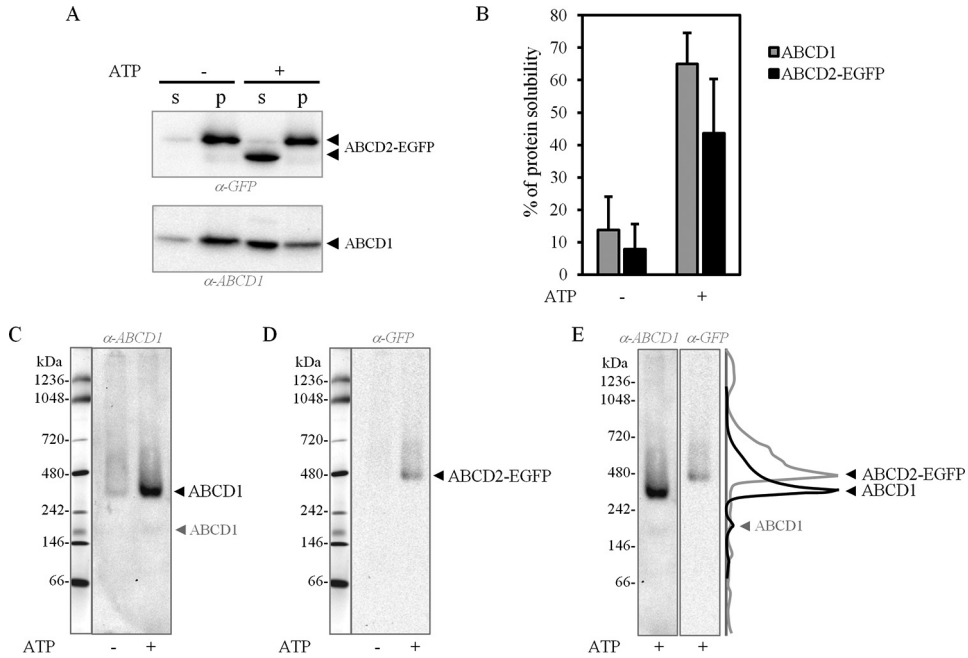

Figure 6. Presence of ABCD1 and ABCD2-EGFP in distinct high-molecular weight complexes in rat hepatoma cells by native PAGE. ABCD1 and ABCD2-EGFP membrane extraction from induced clone 28.38 was performed by α-DDM-containing solubilization buffer on peroxisome-enriched fraction preincubated or not with ATP. *A*, after centrifugation, the resulting soluble (supernatant (*s*)) and insoluble (pellet (*p*)) fractions were analyzed by SDS-PAGE and immunoblotting. Immunoblots are representative of three independent experiments. *B*, histograms representing the densitometric analysis of immunoblots of solubilized ABCD1 and ABCD2-EGFP from the peroxisome-enriched fraction preincubated or not with ATP. A markedly increased solubility of ABCD1 (4.7-fold) and ABCD2-EGFP (5.5-fold) was obtained with ATP. Values are mean ± S.D. (*error bars*) ($n = 6$). *C* and *D*, analysis of the soluble fraction (with/without ATP conditions) by native PAGE. The same PVDF membrane was used for immunoblotting with the anti-ABCD1 antibody (*C*) and with the anti-GFP antibody (*D*) after membrane stripping, to detect ABCD1 and ABCD2-EGFP proteins, respectively. The same native molecular mass marker lane is indicated at the *left*. ABCD1 is detected as a major band at ~350 kDa consistent with tetrameric assembly and as a faint band at ~200 kDa consistent with dimeric assembly. ABCD2-EGFP is only detected as a major band at ~480 kDa consistent with tetrameric assembly. *E*, superimposition of the densitometric tracing of the native-PAGE electrophoretic patterns showed that ABCD1 and ABCD2 were mainly present in distinct complexes, as shown by a weak overlapping of ABCD1 and ABCD2-EGFP bands. The native-PAGE immunoblotting images are representative of several experiments performed.

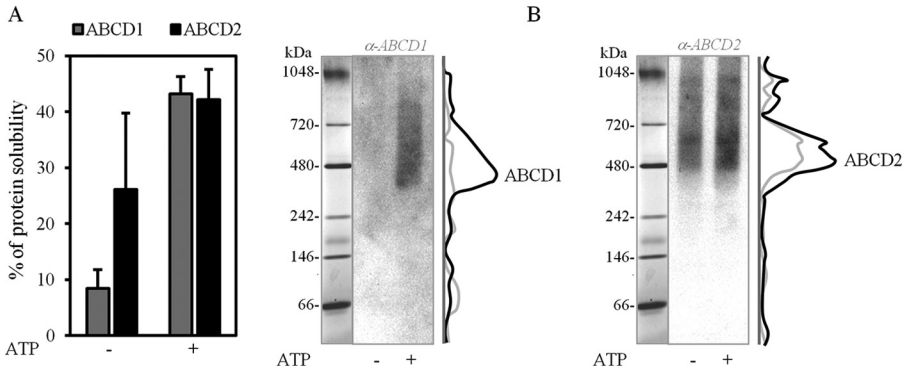

Figure 7. Native-PAGE profiles of ABCD1 and ABCD2 in the BV-2 microglial cell line. *A*, histograms representing the percentage of α-DDM-solubilized ABCD1 and ABCD2 proteins from the BV-2 cell peroxisome-enriched fraction, preincubated or not with ATP. Values are mean ± S.D. (*error bars*) ($n = 3$). The densitometric analyses were performed on immunoblots using the anti-ABCD1 and anti-ABCD2 antibodies. *B*, native-PAGE profiles of solubilized ABCD1 and ABCD2, as described in *A* showed that both proteins are found in high-molecular weight complexes. The same PVDF membrane was used for immunoblotting with the anti-ABCD1 antibody (*left*) and with the anti-GFP antibody (*right*) after membrane stripping. In both *panels*, the same native molecular mass marker lane is indicated at the *left*. ABCD1 is detected in a large band with an estimated molecular mass in the range of 350–700 kDa (*left*). ABCD2 is detected in a large band as well, with an estimated molecular mass in the range of 480–700 kDa (*right*).

mized native-PAGE experiments confirmed that tetrameric assemblies were predominant in ABCD2-EGFP forced expression cells (clone 28.38) and in ABCD1/ABCD2-naturally expressing cells (BV-2) as well. The weak overlap of ABCD1 and ABCD2 bands on native-PAGE profiles indicates that homotetramers are greatly favored over the heterotetramers. Previous bioluminescence resonance energy transfer experiments have led to the conclusion that homo-oligomerization of ABCD1 is favored over hetero-oligomerization with ABCD3 (39). Moreover, ABCD1 homointeraction, interpreted as a dimer, was also found to be either predominant in transfected cells (21) or exclusive in the liver (22), an organ with low ABCD2 expression level (2, 16). Hence, the predominance of homotetramers over heterotetramers is consistent with previous data reporting preferred homointeraction over heterointeraction.

In an attempt to decipher the composition of the tetrameric forms, we took advantage of the C4C8 detergent, which solubilized ABCD1 and ABCD2-EGFP as a mix of monomer/dimer.

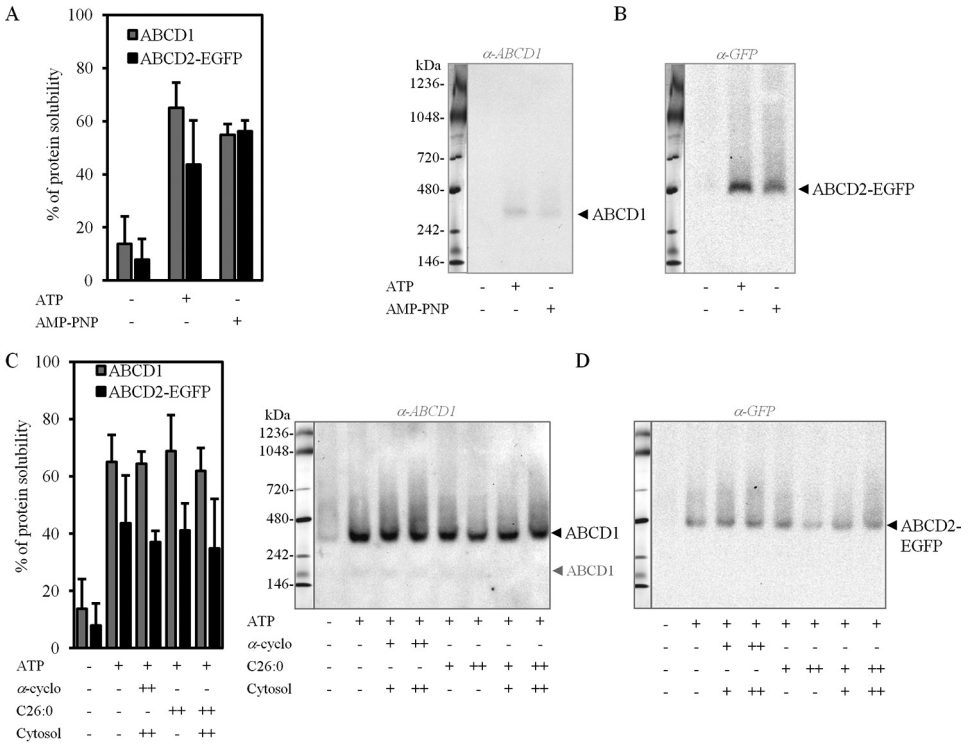

Figure 8. Unchanged ABCD1- and ABCD2-EGFP molecular assemblies during the catalytic cycle of the transporters. *A*, histograms representing the percentage of α-DDM-solubilized ABCD1 and ABCD2-EGFP proteins from the induced clone 28.38 peroxisome-enriched fraction preincubated or not with ATP or AMP-PNP. The densitometric analyses were performed on immunoblots using the anti-ABCD1 and anti-GFP antibodies. Values are mean ± S.D. (*error bars*) ($n = 3$). *B*, native-PAGE profiles of solubilized ABCD1 and ABCD2-EGFP, as described in *A*. The same PVDF membrane was used for immunoblotting with anti-ABCD1 (*left*) and anti-GFP (*right*) antibodies after membrane stripping, and the same native molecular mass marker lane is indicated in both *panels*. The molecular assembly of both proteins remained unchanged whatever the pretreatment done. *C*, histograms representing the densitometric analysis of immunoblots of α-DDM-solubilized ABCD1 and ABCD2-EGFP from the induced clone 28.38 peroxisome-enriched fraction preincubated in the presence of 4 mM ATP (+); 0.2 (+) or 0.8 mM α-cyclodextrine (++); 4 (+) or 16 μM C26:0 (++); or cytosol (++) or 4-fold dilution (+), separately or in combination as indicated. *D*, native-PAGE profiles of solubilized ABCD1 and ABCD2-EGFP, as described in *C*. The same PVDF membrane was used for immunoblotting with anti-ABCD1 (*left*) and anti-GFP (*right*) antibodies, and the same native molecular mass marker lane is indicated at the *left* of both *panels*. The molecular assembly of both proteins (*i.e.* the 350-kDa ABCD1 complex and the 480-kDa ABCD2-EGFP complex) remained unchanged whatever the pretreatment done.

Table 1
List of proteins identified in co-immunoprecipitated ABCD2-EGFP complex by LC-MS/MS

Protein accession	Protein symbol	Protein name	No. of peptides[a]	Protein probability	Sequence coverage	Change[b]
					%	*-fold*
Q9QY44	**ABCD2**	**ATP-binding cassette sub-family D member 2**	**28 (2)**	**1**	**51.7**	**12.42**
P97612	FAAH1	Fatty-acid amide hydrolase 1	4	1	13.1	5.02
P11507	AT2A2	Sarcoplasmic/endoplasmic reticulum calcium ATPase 2	27 (7)	1	34.6	4.71
P07340	AT1B1	Sodium/potassium-transporting ATPase subunit beta-1	3	1	25	2.48
P55159	PON1	Serum paraoxonase/arylesterase 1	9	1	40.8	2.32
D3ZHR2	ABCD1	ATP-binding cassette sub-family D member 1	7 (2)	1	17	< 2
P16970	ABCD3	ATP-binding cassette sub-family D member 3	4	1	11.1	< 2
Q7TS56	CBR4	Carbonyl reductase family member 4	3	1	17.4	< 2
P11505	AT2B1	Plasma membrane calcium-transporting ATPase 1	6 (2)	1	6.6	< 2
P16086	SPTN1	Spectrin α chain, non-erythrocytic 1	8	1	3.9	< 2
Q63151	ACSL3	Long-chain acyl-CoA synthetase 3	3	0.9997	6.9	< 2
O88813	ACSL5	Long-chain acyl-CoA synthetase 5	2	0.9994	3.4	< 2
P14408	FUMH	Fumarate hydratase, mitochondrial	1	0.8013	3.9	< 2
P25235	RPN2	glycosyltransferase subunit 2	1	0.7224	3.8	< 2

[a] Numbers in parentheses refer to the numbers of shared peptides between homologous proteins among the total number of peptides indicated.
[b] Statistical significance was obtained for proteins identified with a -fold change > 2.

This detergent belongs to the anionic calix[4]arene-based detergent described to successfully extract several functional ABC half-transporters as dimers (30). Interestingly, the absence of interaction of ABCD1 with ABCD2-EGFP by co-IP experiments when solubilized with C4C8 suggests that homointeraction is greatly favored or pushed to the extreme that only homointeraction would exist within a dimer. This result calls into question the relevance of the chimeric heterodimers that we previously constructed and studied (24). Despite the fact that the chimeric heterodimers were functionally active, we were intrigued by their much lower expression levels compared with chimeric homodimers. The results observed for chimeric heterodimers after temperature rescue experiments suggest that the low expression level is due to folding defects. Thus, the absence of interaction of ABCD1 with ABCD2 within a dimer, as evidenced by co-IP, suggests that ABCD1/ABCD2 het-

erodimers might not be favored or even might not exist *in vivo*. Hence, the absence of or minor heterointeraction within a dimer and the existence of heterotetramers suggest that heterotetramers would be mainly composed of two different homodimers.

In the ABC field, the structure-function relationship remains difficult to establish for such intractable proteins, and only a few reports have been published. Yang *et al.* (28) succeeded in demonstrating that the functional unit of the full-length transporter ABCC1 involved in multidrug resistance is a dimer, thanks to an ABCC1 mutant that has a dominant-negative function when co-expressed with wild-type ABCC1. Interestingly, for the cholesterol full-length transporter ABCA1, a dimer-monomer interconversion occurred during HDL generation revealed by single-molecule imaging (26). The oligomerization (monomers, dimers, and even tetramers) of the surfactant lipid transporter ABCA3, a full-length ABC, was suggested to be crucial for its function (27). Concerning ABCD1, acyl-CoA binding induced conformational changes, as assessed by a protease-based approach (40). However, these conformational changes probably do not affect the overall molecular assembly of the transporter because the ABCD1 tetrameric assembly remained unchanged during the catalytic cycle. Thus, contrary to ABCA1 and ABCA3, for which both monomeric and oligomeric forms co-exist during the catalytic cycle, ABCD1 and ABCD2 are likely to form obligate tetramers during this cycle.

In ABC transporters, a tight cross-talk between substrate binding and ATP binding has been extensively described and is associated with the modification of the inward/outward-facing structures. Of note, whatever the different biochemical approaches used in our study, difficulties in solubilizing ABC transporters from the peroxisomal membrane were overcome by preincubation of peroxisomes with ATP before the solubilization step. We hypothesized that the difference in solubility could be due to the supposed different conformations adopted by the transporters during the catalytic cycle. Indeed, ABC transporters were described as adopting an inward-facing conformation, with very large separation of the NBDs in the absence of ATP, and an outward-facing conformation with a smaller separation of the NBDs when bound to nucleotides (41). Thus, a transporter in an outward-facing conformation, which is the most compact structure, should be easier to extract from the peroxisomal membrane by the detergent micelle. It could also be postulated that the observed resistance to α-DDM solubilization is related to the association of peroxisomal ABC transporters with detergent-resistant microdomains. In the presence of ATP, both transporters would be distributed outside the detergent-resistant microdomains and hence would be easily solubilizable. ABCD1 and ABCD3 were indeed described as being associated with different detergent-resistant microdomains in peroxisomes of hepatocytes (42). Further experiments should be done to shed light on this increased solubility mediated by ATP, which certainly has a biological relevance.

In any even, the fact that heterotetramers of ABCD1 and ABCD2 would be composed of two different homodimers is of particular interest. In a previous study, we have demonstrated a transdominant-negative effect of mutated ABCD2 on ABCD1 function (8). In light of the current results, it would mean that the functional unit is at minimum a tetramer. If ABCD1 tetramerization is indeed crucial for its function, disruption of oligomerization due to mutations could represent a novel pathomechanism in X-ALD. It is thus important to determine whether ABCD1 mutations that are found in X-ALD patients have any impact on its tetramerization. Among the >300 non-recurrent missense *ABCD1* gene mutations distributed all along the protein sequence, those located in the last 87 C-terminal amino acids could be of interest because this region has been reported to be involved in ABCD1 interaction with itself and with ABCD2 and ABCD3 (19, 21).

The native-PAGE profiles obtained suggest that besides tetrameric forms, higher molecular assemblies of ABCD1 and ABCD2 are present, up to 720 kDa. Coincidently, similar native-PAGE experiments from *Arabidopsis thaliana* cultured cells showed the presence of the unique peroxisomal ABC transporter (*i.e.* COMATOSE, a full-length transporter ortholog to ABCD1) in a complex of ~700 kDa (43). Several studies have reported physical interaction between the peroxisomal ABCD transporters and other proteins, such as the very long-chain acyl-CoA synthetases 1 and 4 (ACSVL1 and -4), the ATP citrate synthase, the fatty-acid synthase variant protein (FASN), the phytanoyl-CoA 2-hydroxylase, and PEX19p (39, 44–46). Large complexes containing ABC transporters and accessory proteins are frequent in the ABC family. Moreover, such interactions are in agreement with the hydrophobic nature of the substrates, which probably require a "continual chaperoning" from the cytosol to the peroxisomal matrix. Among the interacting partners listed above, only PEX19p has been reported to interact with the ABCD2 transporter (46). The co-IP/MS strategy developed in the present study has been adapted to membrane proteins and successfully identified potential binding partners of ABCD2, including soluble and membrane proteins. These partners are different from those previously identified for ABCD1, ABCD2, and ABCD3 (39, 44–46). Interestingly, they are distributed in the peroxisome (ABCD1 and ABCD3) but also in the cytoplasm (spectrin α chain, SPTN1), in lipid droplets (long-chain acyl-CoA synthetase 3 (ACSL3)), and in other organelles, such as endoplasmic reticulum (FAAH1 and long-chain acyl-CoA synthetase 3 (ACSL3)) and mitochondria (carbonyl reductase family member 4 (CBR4) and ACSL5). These data corroborate the existence of peroxisome interconnection with organelles, lipid droplets, and the cytoskeleton (47). The first molecular mechanism for establishing peroxisome-endoplasmic reticulum associations has been discovered recently (48, 49). Moreover, it has been evidenced recently that ABCD2 is localized to a subclass of peroxisome that may associate physically with mitochondria and the endoplasmic reticulum (50). Nevertheless, the mechanisms leading to such physical contacts between these different cell compartments and the physiological relevance of these interactions are largely unknown.

The co-IP/MS experiment succeeded in identifying ABCD1 and ABCD3 proteins as ABCD2-binding partners, despite the presence of degenerate peptides (two shared peptides between ABCD1 and ABCD2), which brings uncertainty and ambiguity in determining the identities of sample proteins (51). The -fold change between samples expressing or not ABCD2-EGFP was

used as a guide for specific interaction. Although ABCD1 and ABCD3 were identified with a -fold change less than the arbitrary threshold value of 2, ABCD1 and ABCD3 are true ABCD2 partners, judging from the present co-IP assays and from previous reports (8, 19, 20, 24).

The protein identified with the highest -fold change is FAAH1 localized at the endoplasmic reticulum and responsible for the degradation of fatty-acid amides to the corresponding fatty acids, with a preference of PUFA over MUFA and saturated fatty acids, at least for the long-chain fatty acids tested (52, 53). As a reminder, ABCD2, but not ABCD1 or ABCD3, would be involved in the transport of PUFA, such as docosahexaenoic acid (DHA) (C22:6 *n*-3) (5, 8). Interestingly, the ethanolamine amide of DHA (*N*-docosahexaenoyl ethanolamine) is degraded to DHA by the FAAH1 (54), and DHA is known to be β-oxidized into the peroxisome (55). Hence, it is tempting to speculate that FAAH1 interaction with ABCD2 permits to supply the PUFA substrate to ABCD2 for further degradation into the peroxisome. Other potential binding partners of ABCD2 identified are involved in lipid metabolism, such as CBR4 and the long-chain acyl-CoA synthetase 3 and 5 (ACSL3 and ACSL5). Interestingly, ACSL3 has a substrate preference for PUFA (56).

AT2A2 was also identified with a high -fold change, suggesting that this protein is also a true interactor of ABCD2. In addition, its homolog (AT2A1) has been identified by proteomic analysis in a subclass of peroxisome expressing ABCD2 (50). By transferring Ca^{2+} from the cytosol to the endoplasmic reticulum, this enzyme is involved in calcium signaling. Interestingly, disturbed calcium signaling was recently proposed to be involved in the pathogenesis of X-ALD (57). Altogether, the link between ABCD2 and calcium signaling would require further investigation, especially because the calcium-transporting ATPase 1 (AT2B1), which is expressed at the plasma membrane and transports calcium out of the cell, was also identified as a potential interactor of ABCD2 (Table 1).

In conclusion, the characterization of the quaternary structure of ABCD1 and its homolog ABCD2 demonstrated for the first time that both proteins exist as tetramers, mainly homotetramers, in the peroxisomal membrane. However, the functional significance of this tetramerization remains unknown. A question that is still pending is whether or not oligomerization participates in substrate specificity. Molecular complexes of higher molecular weight were also observed and remain to be characterized in detail. In addition, we identified potential binding partners of ABCD2, involved in PUFA metabolism and calcium signaling, whose interaction with ABCD2 remains to be confirmed and whose physiological relevance remains to be elucidated.

Experimental procedures

Cell culture

H4IIEC3 rat hepatoma cells stably expressing ABCD2-EGFP (clone 28.38) (8, 31) were cultured as described previously. COS-7 cells (ECACC catalog no. 87021302) were grown in DMEM supplemented with 10% FBS. Murine microglial cells (BV-2) from Banca-Biologica e Cell Factory (catalog no. ATL03001) were cultured in DMEM supplemented with 10% heat-inactivated FBS and 1% penicillin/streptomycin (Dutscher). Cultures were maintained at 37 °C in a humidified atmosphere containing 5% CO_2.

Plasmid constructs

For COS-7 cell transfection, the pEGFP-N3 plasmids coding for the chimeric dimers fused to EGFP (ABCD1-ABCD1-EGFP and ABCD2-ABCD2-EGFP) were obtained previously (24). The pcDNA3.1(−) plasmids coding for ABCD1-ABCD1 and ABCD2-ABCD2 were obtained by a similar strategy (24) and generated chimeric proteins containing two moieties linked by 3 alanine residues.

Transfection

COS-7 cells (500,000 cells at 70–80% confluence) were transiently transfected with plasmids (4 μg for a single transfection or 2 μg of each plasmid for double transfection) coding for the chimeric dimers (pEGFP-N3 or pcDNA3.1(−) plasmids) using the ExGen 500 *in vitro* transfection reagent (Euromedex), according to the manufacturer's instructions. After transfection, cells were cultured in DMEM supplemented with 10% FBS for 48 h and then lysed for further experiments.

Peroxisome-enriched fraction isolation by subcellular fractionation

Cells (from 10 140-mm-diameter Petri dishes at 80–90% confluence) were homogenized in 100 ml of homogenization buffer (HB) (250 mM sucrose, 1 mM EDTA, 0.1% ethanol, 50 mM Tris-HCl, pH 7.5) by six strokes with a Dounce homogenizer (pestle B) followed by centrifugation at 1,000 × *g* for 5 min. The pellet was suspended in HB, and homogenization was repeated twice. Supernatants were pooled and then centrifuged first at 7,500 × *g* for 4 min, 8 s and second at 55,000 × *g* for 4 min, 48 s to pellet peroxisomes, lysosomes, and light mitochondria. After pellet resuspension in 5 ml of HB and protein concentration measurement using the bicinchoninic acid assay (BCA; Sigma-Aldrich), the peroxisome-enriched fraction (L fraction) (58) was subjected to ABCD protein solubilization assays.

Cytosolic fractions were prepared from 8 140-mm-diameter Petri dishes at 80–90% confluence of H4IIEC3 rat hepatoma cells stably expressing ABCD2-EGFP (clone 28.38 + 2 μg/ml doxycycline overnight). Cells were homogenized (Dounce, pestle B) in 2 ml of HB, and the homogenate was centrifuged at 199,000 × *g* for 45 min. The resulting supernatant corresponds to the cytosolic fraction.

ABCD protein solubilization assays from the peroxisome-enriched fraction

The peroxisome-enriched pellet was suspended (20 μg/150 μl) in the treatment buffer (0.25 M sucrose, 10 mM $MgCl_2$, 50 mM Tris-HCl, pH 8.0) containing separately or in combination 4 mM ATP (Sigma-Aldrich), 4 mM AMP-PNP (Sigma-Aldrich), 0.8 mM α-cyclodextrine (Sigma-Aldrich), 4 or 16 μM C26:0, and a 1:5 dilution (+) or 2:5 dilution (++) of the cytosol. The mixture was incubated at 37 °C for 40 min, and after centrifugation at 20,000 × *g* for 20 min, the pellet was suspended in the solubilization buffer (50 mM Tris-HCl, 150 mM NaCl, 0.4% detergent, pH 8.0) for 30 min at 4 °C (15 μl/pellet). After centrifugation (20,000 × *g* for 20 min at 4 °C), the supernatant (containing

solubilized proteins) and/or the pellet (containing insoluble proteins) were either loaded on SDS-PAGE or on native PAGE for further analysis.

Velocity sucrose gradient centrifugation

COS-7 cells transfected with pABCD2-ABCD2-EGFP-N3 plasmid (48 h post-transfection) or H4IIEC3 rat hepatoma cells stably expressing ABCD2-EGFP (clone 28.38 + 2 μg/ml doxycycline overnight) and at 80–90% confluence were washed twice with phosphate-buffered saline (PBS). The cells were then solubilized at 4 °C for 30 min in 150 mM NaCl and 50 mM Tris-HCl, pH 7.4, in the presence of 1% SDS, 1% of the anionic calix[4]arene-based detergent C4C8 (30), 1% Triton X-100 (Euromedex), 1% α-DDM (Anatrace), or 1% β-DDM (Anatrace) and supplemented with a protease inhibitor mixture (Roche Diagnostics) plus 1 mM phenylmethylsulfonyl fluoride (PMSF). After centrifugation at 20,000 $\times$ *g* at 4 °C for 20 min, the cleared post-nuclear supernatant was collected, and protein concentration was measured by BCA. Post-nuclear supernatants (2.5 mg) adjusted to 400 μl were layered on top of a discontinuous 5–30% (w/v) sucrose gradient prepared by successive layers of 2.5 ml of 30% (w/v), 2 ml of 20%, 2 ml of 15%, 2 ml of 10%, and 2 ml of 5% sucrose in 50 mM Tris-HCl (pH 7.4), 150 mM NaCl, and the appropriate detergent. The overlaid gradients were subjected to ultracentrifugation in a SW41 rotor at 260,000 $\times$ *g* for 12 h at 4 °C except for SDS gradients (24 °C). At equilibrium, twenty-two 500-μl fractions were collected and numbered from top to bottom. For sucrose gradients loaded with lysate of ABCD2-ABCD2-EGFP-transfected COS-7 cells, protein samples from each fraction collected were concentrated 5 times by acetone precipitation. Each fraction (50 μl, concentrated or not) was analyzed for ABCD1 and ABCD2 contents by immunoblotting. Sucrose gradient linearity was confirmed by refractometry (Abbe-2WAJ) on blank gradients.

Because the estimation of the approximate molecular weight of membrane protein complexes by comparison with sedimentation of soluble protein standards is complicated by the contribution of unknown amounts of bound detergent in the micelle and by the fact that micelles may affect buoyancy, we included a membrane protein marker, the chimeric dimer ABCD2-ABCD2-EGFP. Native soluble protein markers (thyroglobulin (669 kDa), catalase (232 kDa), β-amylase (200 kDa), conalbumin (75 kDa), ovalbumin (44 kDa)) and a denatured membrane protein marker ABCD2-ABCD2-EGFP (194 kDa) were run in parallel gradients. Peak migration of soluble markers and of the membrane marker was determined by absorbance at 280 nm or by immunoblotting analysis, respectively, for all fractions.

Co-IP assays

Mouse monoclonal anti-GFP antibody covalently immobilized on agarose beads (MBL) and homemade rabbit polyclonal anti-ABCD1 antibody (serum 029) cross-linked to agarose beads via dimethyl pimelimidate (24) were used for co-IP assays. COS-7 cells transiently transfected with plasmids (coding for ABCD1-ABCD1, ABCD1-ABCD1-EGFP, ABCD2-ABCD2, ABCD2-ABCD2-EGFP) and H4IIEC3 cells stably expressing ABCD2-EGFP (clone 28.38 + 2 μg/ml of doxycycline overnight) or not were homogenized in the solubilization buffer: 50 mM Tris-HCl, pH 7.4, 150 mM NaCl, 1% detergent (C4C8 (30), Triton X-100, or β-DDM), 1 mM PMSF, and protease inhibitor mixtures (Roche Diagnostics). Immunoprecipitation assays (from 200 to 1,600 μg of precleared cell lysate) were carried out as described previously (24). Bound proteins, including IP and co-IP proteins, were analyzed by SDS-PAGE, followed by immunoblotting with anti-ABCD1, anti-ABCD2, and anti-GFP antibodies.

For co-IP assays coupled to mass spectrometry, the peroxisome-enriched fractions were prepared as described from the clone 28.38 expressing or not expressing ABCD2-EGFP (with or without 2 μg/ml doxycycline overnight). The α-DDM-soluble fractions of the peroxisome-enriched fraction (300 μg) were subjected to anti-GFP (covalently immobilized on agarose beads (MBL)) co-IP assays. Eluted proteins were further identified by LC-MS/MS.

Native-PAGE fractionation and analysis

Solubilized proteins (with 0.4% α-DDM containing solubilization buffer) from peroxisome-enriched fractions (20 μg/assay) preincubated with fatty acid and/or cytosolic fraction and/or ATP or derivatives were loaded on a Deriphat native PAGE as described previously (36). Samples were fractionated on 4–16% native-PAGE BisTris gel (Life Technologies, Inc.), and 0.1% Deriphat was included in the upper reservoir. After electrophoresis at 4 °C at 50 V for 12 h, proteins were transferred onto a PVDF membrane at 4 °C in 25 mM Tris, 192 mM glycine, and 20% (v/v) methanol. PVDF membranes were further probed with antibodies to detect the presence of ABCD1 and ABCD2 proteins. The migration of native marker unstained protein standards (Invitrogen) was analyzed by Coomassie Brilliant Blue G staining (Sigma-Aldrich) of an excised marker lane of the gel and by Ponceau S staining of the PVDF membrane.

Western blotting

Proteins from total cell lysate (40–50 μg), proteins solubilized or not from peroxisome-enriched fraction (20 μg/assay), velocity sucrose gradient fractions concentrated or not (50 μl), and immunoprecipitated proteins were separated on 7.5% SDS-PAGE or on 4–16% native Deriphat-PAGE and transferred onto a PVDF membrane. First incubated in 5% skimmed milk in PBS, 0.1% Tween 20 (PBS/T) for 1 h at room temperature, the membrane was then probed with mouse anti-β-actin (dilution 1:10,000; Sigma-Aldrich), mouse anti-GFP (dilution 1:250; Roche Diagnostics), rabbit polyclonal anti-ABCD1 (1:5,000; homemade serum 029) (24), or rabbit polyclonal anti-ABCD2 (generous gift from Prof. G. Graf, University of Kentucky) (9) antibodies. The anti-ABCD1 and anti-ABCD2 antibodies do not cross-react with ABCD2 and ABCD1, respectively (data not shown). Following the incubation with the appropriate horseradish peroxidase (HRP)-conjugated secondary antibody (1:5,000; Santa Cruz Biotechnology, Inc.), immunoreactivity was revealed by ECL (Santa Cruz Biotechnology). Image processing and analysis were obtained using a Bio-Rad-Chemidoc XRS system and the Image Lab version 4.0 software for quantitative analysis. The double band detected with the anti-

GFP antibodies on immunoblots obtained from SDS-PAGE corresponds to two different denatured states of the ABCD2-EGFP protein: a fully denatured protein (upper band) and a partially denatured protein (lower band). These two bands were obtained because samples were not boiled to avoid membrane protein aggregation. Both bands were systematically considered when immunoblots were subjected to densitometric analysis.

Protein identification by LC-MS/MS

Eluted proteins from co-IP assays were separated (short gel run, 1 cm) on 1D PAGE (Invitrogen). This 1-cm area was cut in spots and washed with 0.1 M NH_4HCO_3 and next with 100% acetonitrile (ACN) for 10 min. Reduction/alkylation was achieved by incubating the excised spots successively in 10 mM tris(2-carboxyethyl) phosphine, 0.1 M NH_4HCO_3 for 30 min at 37 °C and in 55 mM iodoacetamide, 0.1 M NH_4HCO_3 for 20 min. Peptide fragments were obtained after digestion with a solution of 40 mM NH_4HCO_3, 10% ACN containing 5 ng/μl trypsin (Promega) for 3 h at 37 °C. The resulting peptides were acidified with 0.1% formic acid. Extraction from the polyacrylamide gel pieces was performed by two successive incubations for a few min in ACN with sonication.

Peptides were further concentrated by evaporation and separated with the Ultimate 3000 RSLC nano system (ThermoScientific) fitted with a C18 trapping column (5-μm average particle diameter; 300-μm inner diameter × 5-mm length; ThermoScientific) and a C18 analytical column (2-μm average particle diameter, 75-μm inner diameter × 150-mm length; ThermoScientific). A 120-min gradient was performed, and peptides were analyzed by nano-LC-MS/MS using an LTQ-Orbitrap Elite mass spectrometer equipped with the Advion TriVersa NanoMate nanospray source. Full-scan spectra from a mass/charge ratio of 400 to one of 1,700 at a resolution of 120,000 full width at half-maximum were acquired in the Orbitrap mass spectrometer. From each full-scan spectrum, the 20 ions with the highest intensity were selected for fragmentation in the ion trap, and a 30-s exclusion time was defined. Each sample was analyzed in triplicate.

The acquired data were searched against the International Protein Index/UniProt using Mascot and X!Tandem. Based on tandem mass spectrometry data, peptide and protein identifications were validated through Peptide and ProteinProphet software (59). At the end of the above steps, each injection was described by a list of validated proteins and peptides. Peptides that were not identified in at least 2 of the 3 technical replicates injected per sample were excluded. Retention times were then aligned, and peptide intensity was extracted using the MASIC software (60). Using this quantification, a new filter based on the coefficients of variation of each peptide in each sample is applied to discard too poorly reproducible peptides. A linear mixed model is then used to select differential proteins between the positive (+dox) and negative (−dox) conditions (61). The false-discovery rate correction was applied to take into account the high dimension (far more tested variables than samples). Proteins identified with a -fold change higher than 2, with a false-discovery rate at 5%, were kept. Proteins detected exclusively in the positive samples but absent in the negative samples are also listed even if their presence is not statistically relevant.

Author contributions—F. G., C. G., and D. T. designed the experiments. F. G. conducted most of the experiments. C. G., Q. R., and A. M. M. D. participated in the biochemical data collection. D. P., C. T., G. L., and P. D. designed and performed mass spectrometry analyses. P. F. provided calixar detergents. F. G., C. G., S. S., D. T. analyzed data. D. T. conceived and coordinated the study with S. S. S. S. and D. T. wrote the paper. All authors read, improved, and approved the final manuscript.

Acknowledgments—We thank Thomas Munch, Lucine Marotte, and Stéphanie Nguyen for technical assistance as master student trainees.

References

1. Mosser, J., Douar, A. M., Sarde, C. O., Kioschis, P., Feil, R., Moser, H., Poustka, A. M., Mandel, J. L., and Aubourg, P. (1993) Putative X-linked adrenoleukodystrophy gene shares unexpected homology with ABC transporters. *Nature* **361,** 726–730
2. Trompier, D., and Savary, S. (2013) *X-linked Adrenoleukodystrophy*, Morgan & Claypool Life Sciences, 10.4199/C00075ED1V01Y201303GBD004
3. Wiesinger, C., Kunze, M., Regelsberger, G., Forss-Petter, S., and Berger, J. (2013) Impaired very long-chain acyl-CoA β-oxidation in human X-linked adrenoleukodystrophy fibroblasts is a direct consequence of ABCD1 transporter dysfunction. *J. Biol. Chem.* **288,** 19269–19279
4. van Roermund, C. W., Visser, W. F., Ijlst, L., van Cruchten, A., Boek, M., Kulik, W., Waterham, H. R., and Wanders, R. J. (2008) The human peroxisomal ABC half transporter ALDP functions as a homodimer and accepts acyl-CoA esters. *FASEB J.* **22,** 4201–4208
5. van Roermund, C. W., Visser, W. F., Ijlst, L., Waterham, H. R., and Wanders, R. J. (2011) Differential substrate specificities of human ABCD1 and ABCD2 in peroxisomal fatty acid β-oxidation. *Biochim. Biophys. Acta* **1811,** 148–152
6. Lombard-Platet, G., Savary, S., Sarde, C. O., Mandel, J. L., and Chimini, G. (1996) A close relative of the adrenoleukodystrophy (ALD) gene codes for a peroxisomal protein with a specific expression pattern. *Proc. Natl. Acad. Sci. U.S.A.* **93,** 1265–1269
7. Kamijo, K., Taketani, S., Yokota, S., Osumi, T., and Hashimoto, T. (1990) The 70-kDa peroxisomal membrane protein is a member of the Mdr (P-glycoprotein)-related ATP-binding protein superfamily. *J. Biol. Chem.* **265,** 4534–4540
8. Genin, E. C., Geillon, F., Gondcaille, C., Athias, A., Gambert, P., Trompier, D., and Savary, S. (2011) Substrate specificity overlap and interaction between adrenoleukodystrophy protein (ALDP/ABCD1) and adrenoleukodystrophy-related protein (ALDRP/ABCD2). *J. Biol. Chem.* **286,** 8075–8084
9. Liu, J., Sabeva, N. S., Bhatnagar, S., Li, X. A., Pujol, A., and Graf, G. A. (2010) ABCD2 is abundant in adipose tissue and opposes the accumulation of dietary erucic acid (C22:1) in fat. *J. Lipid Res.* **51,** 162–168
10. van Roermund, C. W., Ijlst, L., Wagemans, T., Wanders, R. J., and Waterham, H. R. (2014) A role for the human peroxisomal half-transporter ABCD3 in the oxidation of dicarboxylic acids. *Biochim. Biophys. Acta* **1841,** 563–568
11. Ferdinandusse, S., Jimenez-Sanchez, G., Koster, J., Denis, S., Van Roermund, C. W., Silva-Zolezzi, I., Moser, A. B., Visser, W. F., Gulluoglu, M., Durmaz, O., Demirkol, M., Waterham, H. R., Gökcay, G., Wanders, R. J., and Valle, D. (2015) A novel bile acid biosynthesis defect due to a deficiency of peroxisomal ABCD3. *Hum. Mol. Genet.* **24,** 361–370
12. Netik, A., Forss-Petter, S., Holzinger, A., Molzer, B., Unterrainer, G., and Berger, J. (1999) Adrenoleukodystrophy-related protein can compensate functionally for adrenoleukodystrophy protein deficiency (X-ALD): implications for therapy. *Hum. Mol. Genet.* **8,** 907–913
13. Pujol, A., Ferrer, I., Camps, C., Metzger, E., Hindelang, C., Callizot, N., Ruiz, M., Pàmpols, T., Giròs, M., and Mandel, J. L. (2004) Functional

overlap between ABCD1 (ALD) and ABCD2 (ALDR) transporters: a therapeutic target for X-adrenoleukodystrophy. *Hum. Mol. Genet.* **13,** 2997–3006
14. Flavigny, E., Sanhaj, A., Aubourg, P., and Cartier, N. (1999) Retroviral-mediated adrenoleukodystrophy-related gene transfer corrects very long chain fatty acid metabolism in adrenoleukodystrophy fibroblasts: implications for therapy. *FEBS Lett.* **448,** 261–264
15. Troffer-Charlier, N., Doerflinger, N., Metzger, E., Fouquet, F., Mandel, J. L., and Aubourg, P. (1998) Mirror expression of adrenoleukodystrophy and adrenoleukodystrophy related genes in mouse tissues and human cell lines. *Eur. J. Cell Biol.* **75,** 254–264
16. Berger, J., Albet, S., Bentejac, M., Netik, A., Holzinger, A., Roscher, A. A., Bugaut, M., and Forss-Petter, S. (1999) The four murine peroxisomal ABC-transporter genes differ in constitutive, inducible and developmental expression. *Eur. J. Biochem.* **265,** 719–727
17. Langmann, T., Mauerer, R., Zahn, A., Moehle, C., Probst, M., Stremmel, W., and Schmitz, G. (2003) Real-time reverse transcription-PCR expression profiling of the complete human ATP-binding cassette transporter superfamily in various tissues. *Clin. Chem.* **49,** 230–238
18. Trompier, D., Gondcaille, C., Lizard, G., and Savary, S. (2014) Regulation of the adrenoleukodystrophy-related gene (ABCD2): focus on oxysterols and LXR antagonists. *Biochem. Biophys. Res. Commun.* **446,** 651–655
19. Liu, L. X., Janvier, K., Berteaux-Lecellier, V., Cartier, N., Benarous, R., and Aubourg, P. (1999) Homo- and heterodimerization of peroxisomal ATP-binding cassette half-transporters. *J. Biol. Chem.* **274,** 32738–32743
20. Smith, K. D., Kemp, S., Braiterman, L. T., Lu, J. F., Wei, H. M., Geraghty, M., Stetten, G., Bergin, J. S., Pevsner, J., and Watkins, P. A. (1999) X-linked adrenoleukodystrophy: genes, mutations, and phenotypes. *Neurochem. Res.* **24,** 521–535
21. Hillebrand, M., Verrier, S. E., Ohlenbusch, A., Schäfer, A., Söling, H. D., Wouters, F. S., and Gärtner, J. (2007) Live cell FRET microscopy: homo- and heterodimerization of two human peroxisomal ABC transporters, the adrenoleukodystrophy protein (ALDP, ABCD1) and PMP70 (ABCD3). *J. Biol. Chem.* **282,** 26997–27005
22. Guimarães, C. P., Domingues, P., Aubourg, P., Fouquet, F., Pujol, A., Jimenez-Sanchez, G., Sá-Miranda, C., and Azevedo, J. E. (2004) Mouse liver PMP70 and ALDP: homomeric interactions prevail *in vivo*. *Biochim. Biophys. Acta* **1689,** 235–243
23. Tanaka, A. R., Tanabe, K., Morita, M., Kurisu, M., Kasiwayama, Y., Matsuo, M., Kioka, N., Amachi, T., Imanaka, T., and Ueda, K. (2002) ATP binding/hydrolysis by and phosphorylation of peroxisomal ATP-binding cassette proteins PMP70 (ABCD3) and adrenoleukodystrophy protein (ABCD1). *J. Biol. Chem.* **277,** 40142–40147
24. Geillon, F., Gondcaille, C., Charbonnier, S., Van Roermund, C. W., Lopez, T. E., Dias, A. M., Pais de Barros, J. P., Arnould, C., Wanders, R. J., Trompier, D., and Savary, S. (2014) Structure-function analysis of peroxisomal ATP-binding cassette transporters using chimeric dimers. *J. Biol. Chem.* **289,** 24511–24520
25. Wong, K., Briddon, S. J., Holliday, N. D., and Kerr, I. D. (2016) Plasma membrane dynamics and tetrameric organisation of ABCG2 transporters in mammalian cells revealed by single particle imaging techniques. *Biochim. Biophys. Acta* **1863,** 19–29
26. Nagata, K. O., Nakada, C., Kasai, R. S., Kusumi, A., and Ueda, K. (2013) ABCA1 dimer-monomer interconversion during HDL generation revealed by single-molecule imaging. *Proc. Natl. Acad. Sci. U.S.A.* **110,** 5034–5039
27. Frixel, S., Lotz-Havla, A. S., Kern, S., Kaltenborn, E., Wittmann, T., Gersting, S. W., Muntau, A. C., Zarbock, R., and Griese, M. (2016) Homooligomerization of ABCA3 and its functional significance. *Int. J. Mol. Med.* **38,** 558–566
28. Yang, Y., Liu, Y., Dong, Z., Xu, J., Peng, H., Liu, Z., and Zhang, J. T. (2007) Regulation of function by dimerization through the amino-terminal membrane-spanning domain of human ABCC1/MRP1. *J. Biol. Chem.* **282,** 8821–8830
29. Li, C., Roy, K., Dandridge, K., and Naren, A. P. (2004) Molecular assembly of cystic fibrosis transmembrane conductance regulator in plasma membrane. *J. Biol. Chem.* **279,** 24673–24684
30. Matar-Merheb, R., Rhimi, M., Leydier, A., Huché, F., Galián, C., Desuzinges-Mandon, E., Ficheux, D., Flot, D., Aghajari, N., Kahn, R., Di Pietro, A., Jault, J. M., Coleman, A. W., and Falson, P. (2011) Structuring detergents for extracting and stabilizing functional membrane proteins. *PLoS One* **6,** e18036
31. Gueugnon, F., Volodina, N., Taouil, J. E., Lopez, T. E., Gondcaille, C., Grand, A. S., Mooijer, P. A., Kemp, S., Wanders, R. J., and Savary, S. (2006) A novel cell model to study the function of the adrenoleukodystrophy-related protein. *Biochem. Biophys. Res. Commun.* **341,** 150–157
32. Abel, S., Dupradeau, F. Y., Raman, E. P., MacKerell, A. D., Jr., and Marchi, M. (2011) Molecular simulations of dodecyl-beta-maltoside micelles in water: influence of the headgroup conformation and force field parameters. *J. Phys. Chem. B* **115,** 487–499
33. Nury, T., Zarrouk, A., Ragot, K., Debbabi, M., Riedinger, J. M., Vejux, A., Aubourg, P., and Lizard, G. (2016) 7-Ketocholesterol is increased in the plasma of X-ALD patients and induces peroxisomal modifications in microglial cells: potential roles of 7-ketocholesterol in the pathophysiology of X-ALD. *J. Steroid Biochem. Mol. Biol.* 10.1016/j.jsbmb.2016.03.037
34. Niepmann, M., and Zheng, J. (2006) Discontinuous native protein gel electrophoresis. *Electrophoresis* **27,** 3949–3951
35. Peter, G. F., and Thornber, J. P. (1991) Biochemical composition and organization of higher plant photosystem II light-harvesting pigment-proteins. *J. Biol. Chem.* **266,** 16745–16754
36. Trompier, D., Alibert, M., Davanture, S., Hamon, Y., Pierres, M., and Chimini, G. (2006) Transition from dimers to higher oligomeric forms occurs during the ATPase cycle of the ABCA1 transporter. *J. Biol. Chem.* **281,** 20283–20290
37. Shani, N., Sapag, A., Watkins, P. A., and Valle, D. (1996) An S. cerevisiae peroxisomal transporter, orthologous to the human adrenoleukodystrophy protein, appears to be a heterodimer of two half ABC transporters: Pxa1p and Pxa2p. *Ann. N.Y. Acad. Sci.* **804,** 770–772
38. Hettema, E. H., van Roermund, C. W., Distel, B., van den Berg, M., Vilela, C., Rodrigues-Pousada, C., Wanders, R. J., and Tabak, H. F. (1996) The ABC transporter proteins Pat1 and Pat2 are required for import of long-chain fatty acids into peroxisomes of *Saccharomyces cerevisiae*. *EMBO J.* **15,** 3813–3822
39. Hillebrand, M., Gersting, S. W., Lotz-Havla, A. S., Schäfer, A., Rosewich, H., Valerius, O., Muntau, A. C., and Gärtner, J. (2012) Identification of a new fatty acid synthesis-transport machinery at the peroxisomal membrane. *J. Biol. Chem.* **287,** 210–221
40. Guimarães, C. P., Sá-Miranda, C., and Azevedo, J. E. (2005) Probing substrate-induced conformational alterations in adrenoleukodystrophy protein by proteolysis. *J. Hum. Genet.* **50,** 99–105
41. Locher, K. P. (2016) Mechanistic diversity in ATP-binding cassette (ABC) transporters. *Nat. Struct. Mol. Biol.* **23,** 487–493
42. Woudenberg, J., Rembacz, K. P., Hoekstra, M., Pellicoro, A., van den Heuvel, F. A., Heegsma, J., van Ijzendoorn, S. C., Holzinger, A., Imanaka, T., Moshage, H., and Faber, K. N. (2010) Lipid rafts are essential for peroxisome biogenesis in HepG2 cells. *Hepatology* **52,** 623–633
43. De Marcos Lousa, C., van Roermund, C. W., Postis, V. L., Dietrich, D., Kerr, I. D., Wanders, R. J., Baldwin, S. A., Baker, A., and Theodoulou, F. L. (2013) Intrinsic acyl-CoA thioesterase activity of a peroxisomal ATP binding cassette transporter is required for transport and metabolism of fatty acids. *Proc. Natl. Acad. Sci. U.S.A.* **110,** 1279–1284
44. Makkar, R. S., Contreras, M. A., Paintlia, A. S., Smith, B. T., Haq, E., and Singh, I. (2006) Molecular organization of peroxisomal enzymes: protein-protein interactions in the membrane and in the matrix. *Arch. Biochem. Biophys.* **451,** 128–140
45. Ewing, R. M., Chu, P., Elisma, F., Li, H., Taylor, P., Climie, S., McBroom-Cerajewski, L., Robinson, M. D., O'Connor, L., Li, M., Taylor, R., Dharsee, M., Ho, Y., Heilbut, A., Moore, L., *et al.* (2007) Large-scale mapping of human protein-protein interactions by mass spectrometry. *Mol. Syst. Biol.* **3,** 89
46. Gloeckner, C. J., Mayerhofer, P. U., Landgraf, P., Muntau, A. C., Holzinger, A., Gerber, J. K., Kammerer, S., Adamski, J., and Roscher, A. A. (2000) Human adrenoleukodystrophy protein and related peroxisomal ABC transporters interact with the peroxisomal assembly protein PEX19p. *Biochem. Biophys. Res. Commun.* **271,** 144–150

47. Schrader, M., Grille, S., Fahimi, H. D., and Islinger, M. (2013) Peroxisome interactions and cross-talk with other subcellular compartments in animal cells. *Subcell. Biochem.* **69,** 1–22
48. Costello, J. L., Castro, I. G., Hacker, C., Schrader, T. A., Metz, J., Zeuschner, D., Azadi, A. S., Godinho, L. F., Costina, V., Findeisen, P., Manner, A., Islinger, M., and Schrader, M. (2017) ACBD5 and VAPB mediate membrane associations between peroxisomes and the ER. *J. Cell Biol.* **216,** 331–342
49. Hua, R., Cheng, D., Coyaud, É., Freeman, S., Di Pietro, E., Wang, Y., Vissa, A., Yip, C. M., Fairn, G. D., Braverman, N., Brumell, J. H., Trimble, W. S., Raught, B., and Kim, P. K. (2017) VAPs and ACBD5 tether peroxisomes to the ER for peroxisome maintenance and lipid homeostasis. *J. Cell Biol.* **216,** 367–377
50. Liu, X., Liu, J., Lester, J. D., Pijut, S. S., and Graf, G. A. (2015) ABCD2 identifies a subclass of peroxisomes in mouse adipose tissue. *Biochem. Biophys. Res. Commun.* **456,** 129–134
51. Huang, T., Wang, J., Yu, W., and He, Z. (2012) Protein inference: a review. *Brief. Bioinform.* **13,** 586–614
52. Boger, D. L., Fecik, R. A., Patterson, J. E., Miyauchi, H., Patricelli, M. P., and Cravatt, B. F. (2000) Fatty acid amide hydrolase substrate specificity. *Bioorg. Med. Chem. Lett.* **10,** 2613–2616
53. Wei, B. Q., Mikkelsen, T. S., McKinney, M. K., Lander, E. S., and Cravatt, B. F. (2006) A second fatty acid amide hydrolase with variable distribution among placental mammals. *J. Biol. Chem.* **281,** 36569–36578
54. Brown, I., Cascio, M. G., Wahle, K. W., Smoum, R., Mechoulam, R., Ross, R. A., Pertwee, R. G., and Heys, S. D. (2010) Cannabinoid receptor-dependent and -independent anti-proliferative effects of ω-3 ethanolamides in androgen receptor-positive and -negative prostate cancer cell lines. *Carcinogenesis* **31,** 1584–1591
55. Madsen, L., Frøyland, L., Dyrøy, E., Helland, K., and Berge, R. K. (1998) Docosahexaenoic and eicosapentaenoic acids are differently metabolized in rat liver during mitochondria and peroxisome proliferation. *J. Lipid Res.* **39,** 583–593
56. Van Horn, C. G., Caviglia, J. M., Li, L. O., Wang, S., Granger, D. A., and Coleman, R. A. (2005) Characterization of recombinant long-chain rat acyl-CoA synthetase isoforms 3 and 6: identification of a novel variant of isoform 6. *Biochemistry* **44,** 1635–1642
57. Kruska, N., Schönfeld, P., Pujol, A., and Reiser, G. (2015) Astrocytes and mitochondria from adrenoleukodystrophy protein (ABCD1)-deficient mice reveal that the adrenoleukodystrophy-associated very long-chain fatty acids target several cellular energy-dependent functions. *Biochim. Biophys. Acta* **1852,** 925–936
58. De Duve, C., Pressman, B. C., Gianetto, R., Wattiaux, R., and Appelmans, F. (1955) Tissue fractionation studies. 6. Intracellular distribution patterns of enzymes in rat-liver tissue. *Biochem. J.* **60,** 604–617
59. Nesvizhskii, A. I., Keller, A., Kolker, E., and Aebersold, R. (2003) A statistical model for identifying proteins by tandem mass spectrometry. *Anal. Chem.* **75,** 4646–4658
60. Monroe, M. E., Shaw, J. L., Daly, D. S., Adkins, J. N., and Smith, R. D. (2008) MASIC: a software program for fast quantitation and flexible visualization of chromatographic profiles from detected LC-MS(/MS) features. *Comput. Biol. Chem.* **32,** 215–217
61. Clough, T., Thaminy, S., Ragg, S., Aebersold, R., and Vitek, O. (2012) Statistical protein quantification and significance analysis in label-free LC-MS experiments with complex designs. *BMC Bioinformatics* 10.1186/1471-2105-13-S16-S6